Shortened title: HEAVY GAS SIMULATION

Title: NUMERICAL SIMULATION OF INTERACTION OF THE HEAVY GAS CLOUD WITH THE ATMOSPHERIC SURFACE LAYER

Authors: I.V. Kovalets, V.S. Maderich

Affiliations: Institute of Mathematical Machine & System Problems WITH THE ATMOSPHERIC SURFACE LAYER

Address:

Glushkova av. 42

Kiev 03187

Ukraine

Phone: 38-044-5266187

Fax: 38-44-5263615

Email: **vlad@env.kiev.ua**

Citation: Environmental Fluid Mechanics Volume 6, Number 4 (2006), 313-340,
DOI: 10.1007/s10652-005-4288-4

Abstract:

The numerical time-dependent three-dimensional model (Kovalets and Maderich [24]) of the heavy gas dispersion in the atmospheric boundary layer has been improved by parameterizing momentum and heat fluxes on the surface of Earth using Monin-Obukhov similarity theory. Three parameterizations of heat exchange with the surface of Earth were considered: (A) formula of Yaglom and Kader [37] for forced convection, (B) interpolation formula for mixed convection and (C) similarity relationship for mixed convection (Kader and Yaglom [36]). Two case studies were considered. In the first study based on experiment of Zhu *et al*. [4], the interaction of an isothermal heavy gas plume with an atmospheric surface layer was simulated. It was found that stable stratification in the cloud essentially suppresses the turbulence in the plume, reducing the turbulent momentum flux by a factor of down to 1/5 in comparison with the undisturbed value. This reduction essentially influences velocities in the atmospheric boundary layer above the cloud, increasing the mean velocity by a factor of up to 1.3 in comparison with the undisturbed value. A simulation of cold heavy gas dispersion was carried out in the second case based on field experiment BURRO 8. It was shown that both forced and free convections under moderate wind speeds significantly influence the plume. The relative rms and bias errors of prediction the plume's height were $\sigma_H \approx 30\%$ and $\varepsilon_H = -10\%$ respectively for parameterization B, while for A and C the errors were $\sigma_H \approx 80\%$ and $\varepsilon_H \approx -65\%$. It is therefore advised to use the simple parameterization B in dense gas dispersion models.

Key Words: heavy gas dispersion, stratified flows, Richardson number, mixed convection, splitting methods

Abbreviations:

LNG – liquefied natural gas, TKE – turbulent kinetic energy, MOST - Monin-Obukhov similarity theory

1. Introduction

Clouds of hazardous gases can appear as a consequence of emergencies during production, transportation and storage of chemicals in gaseous or liquefied form. The released gas is usually denser than the ambient air because of differences in molecular weight and temperature, as well as presence of liquid aerosol and/or condensed water vapour. The density difference near the source can be comparable with air density. Buoyancy forces, advection by wind and mixing by the ambient turbulence are key factors in the dispersion of the heavy gas (Britter [1]). The buoyancy forces reduce turbulent exchange in the cloud and increase lateral spread of the cloud in a form of density current. The relief of the area and presence of obstacles can also affect movement and dilution of the cloud. Heat exchange of the cloud with the underlying surface is essential for the dispersion of the cold heavy gas clouds (Nielsen and Ott [2]). The buoyancy forces in the cold cloud decrease or even change their sign when influenced by turbulent mixing and heating from the underlying surface. As a result, the initially heavy cloud lifts off the ground (Meroney and Neff [3]). Finally, the gas moves as a neutrally buoyant gas. Under low wind conditions and/or large density differences, the density current covers roughness elements on the surface. Stable stratification in the upper boundary of the cloud can suppress the ambient turbulence, even resulting in laminarization of the cloud (Zhu *et al.* [4], Ding *et al*. [5], Briggs *et al*. [6]). Therefore, an effective roughness of the underlying surface can be reduced. This effect is reflected in the structure of the turbulent surface layer and further in the cloud dispersion.

Models of different complexity were developed for calculation of heavy gas dispersion (see reviews of Meroney [7], Britter [1], Koopman *et al*. [8], Hanna *et al.* [9]). The puff/plume models (e.g. ALOHA (Evans [10]), HEGADAS (Witlox [11]) and SCIPUFF (Sykes *et al.* [12]) are mostly intended for the use in real-time emergency situations, while elaborated 2D shallow layer models (e.g. TWODEE (Hankin and Britter [13]), DISPLAY-2

(Venetsanos *et al.* [14]) are suitable for risk studies, reconstruction of past accidents and emergency response planning, since they can deal with complex terrains. The 3D models (e.g. Edigarov [15], Bartzis *et al*. [16], Pereira and Chen [17], Chan [18]) are considered to be most suitable for reconstruction of past accidents and basic research (i.e. studies of specific processes in the presence of dense cloud, validation of different parameterizations), since they incorporate fewer assumptions and physical restrictions in comparison with simplified models. These models appear to be most appropriate for investigation of the physics of dense gas cloud interaction with the turbulent surface layer, because they do not contain the following important assumptions used in simple models: (i) Assumption about velocity of the gravity current (Britter [1]) which follows from the Boussinesq approximation. This assumption is not valid near the source where density difference can be comparable with air density, Therefore, it results in overestimation of the front passage time (Konig-Langlo and Shatzmann [19]); (ii) Assumptions about entrainment velocity (reviewed in Meroney [7]) are valid only for gravity current in a calm environment, whereas entrainment of dense gas into the atmosphere (extrainment) can exist in a turbulent environment (Nettervile, [20]); (iii) Assumptions about the form of analytical functions for calculating the vertical profile of concentration from the averaged concentration of the layer are in fact not universal (Zhu *et al*. [4]). Most importantly, even 2D models cannot describe the backward influence of the dense gas cloud on characteristics of the atmospheric surface layer.

Accurate modeling of dense gas dispersion is complicated by the fact that the Boussinesq approximation is not applicable at the initial stage of the dense gas dispersion near the source, due to large initial variations of density. Hence, the unfiltered system of gas dynamics equations has to be solved and complexities caused by severe restrictions on the integration time step arise (Patankar [21]). In order to overcome these restrictions one can use fully implicit numerical schemes combined with the splitting method (Kovenya and Yanenko,

[22]). This approach was used by Edigarov [15] and Kovalets and Maderich [23]. In both models the equations of mass and momentum conservation were supplemented by an equation for enthalpy. Turbulence closure in Kovalets and Maderich [23] was performed using an equation for turbulent kinetic energy and algebraic expression for the turbulence length scale. Instead of using the equation for enthalpy, Kovalets and Maderich [24] used an equation for pressure derived from the equation of conservation of internal energy, together with an equation of state for the ideal gas. Such approach has certain advantages when splitting schemes are used for numerical integration. In addition, the $k-\varepsilon$ model was used, which has advantages under highly non-stationary conditions. In both papers of Kovalets and Maderich [23, 24], the models were verified against laboratory and field data on isothermal instantaneous heavy gas releases in the calm environment.

Several experimental data sets were created for the validation of the models of dense gas dispersion, for example, the Thorney Island field experiments (McQuaid and Roebuck [25]) and Kit Fox experiment (WRI [26]). In those experiments, instantaneous and finite duration isothermal releases of dense gas on the flat terrain covered by artificial roughness elements were studied. In BURRO (Koopman *et al*. [8]) and COYOTE (Goldwire *et al*. [28]) field experiments, dispersion of finite duration releases of the liquefied natural gas (LNG) was investigated. Aerosol dispersion was studied in Desert Tortoise experiment with ammonia and in GOLDFISH experiment with hydrofluoric acid HF (Hanna *et al*., [29]) .

The objectives of the present paper are (i) improvement of the 3D model of Kovalets and Maderich [24] with an emphasis on parameterization of momentum and heat fluxes on the Earth's surface and (ii) modeling of two case studies. In the first study, interaction of isothermal heavy gas plume with the atmospheric surface layer will be investigated. The well documented experiment of Zhu *et al.* [4] with continuous isothermal release of CO_2 in the wind tunnel will be simulated in order to demonstrate capability of the 3D model to describe

influence of the dense gas cloud on the turbulence characteristics and mean velocities in the surface layer. In the second case study, influence of mixed convection on the dynamics of the gas cloud and the cooling of subsurface layer will be investigated under the conditions of BURRO 8 experiment. The reason for this choice was the need of data on continuous releases without aerosol fraction from a well defined source (a pool with boiling LNG) with detailed background information.

The paper is organized as follows. In the ensuing section the model and numerical solution techniques are described. In Section 3, the results of simulation of isothermal and cold heavy gas plumes in the turbulent surface layer are compared with the laboratory experiment of Zhu *et al*. [4] and BURRO field trial (Koopman et *al.* [27]).

2. Model

2.1 Governing equations

The 3D time-dependent system of equations describing the turbulent motion of the heavy gas cloud under large Reynolds numbers can be written as follows:

$$\frac{\partial \overline{\rho}}{\partial t} + \frac{\partial (\overline{\rho} \langle u_\alpha \rangle)}{\partial x_\alpha} = 0 , \tag{1}$$

$$\frac{\partial \langle u_i \rangle}{\partial t} + u_j \frac{\partial \langle u_i \rangle}{\partial x_j} + \frac{1}{\overline{\rho}} \frac{\partial}{\partial x_j} \overline{\rho} \left\langle u_i^{"} u_j^{"} \right\rangle + \frac{1}{\overline{\rho}} \frac{\partial \overline{P}}{\partial x_j} = -\delta_{i3} g , \tag{2}$$

$$\frac{\partial \overline{P}}{\partial t} + \langle u_\alpha \rangle \frac{\partial \overline{P}}{\partial x_\alpha} + \frac{\partial}{\partial x_\alpha} \overline{\rho} \left\langle u_\alpha^{"} \Phi^{"} \right\rangle + \overline{\rho} \left\langle c_s^2 \right\rangle \frac{\partial \langle u_\alpha \rangle}{\partial x_\alpha} = 0 , \tag{3}$$

$$\frac{\partial \overline{\rho} \langle C \rangle}{\partial t} + \frac{\partial (\overline{\rho} \langle C \rangle \langle u_\alpha \rangle)}{\partial x_\alpha} + \frac{\partial}{\partial x_\alpha} \overline{\rho} \left\langle u_\alpha^{"} C^{"} \right\rangle = 0 , \tag{4}$$

where t is time, $x_i = (x, y, z)$ are coordinates with $i = 1,2,3$, axis z is directed vertically up from the Earth's surface, ρ is the density, $\langle u_i \rangle = (u, v, w)$ are components of the mean velocity vector, P is the pressure, $c_s = (1/\overline{\rho})(\partial \overline{P} / \partial \overline{\rho})_s$ is the sound speed , C is the mass concentration of the gas, g is the gravity acceleration, $\Phi = P/\rho$, δ_{ij} is the Kronecker delta function. The primed and doubly primed symbols indicate the Reynolds and Favre fluctuations, respectively, $u_i^{"} = \left(u^{"}, v^{"}, w^{"}\right)$. The system of equations (1)-(4) is supplemented with the state equation for the ideal gas:

$$\overline{P} = \overline{\rho}\left(R_a(1 - \langle C \rangle) + R_g \langle C \rangle\right)\langle T \rangle, \tag{5}$$

where R_a, R_g are gas constants for the ambient air and gas, respectively.

Unlike the models of stratified flows with small density deviations, for which the Boussinesq approximation is applicable, the development of models of turbulence for the flows with large deviations of density is far from satisfactory (Jones [31], Sarkar and Lakshmanan [32], Adumitroaie *et al*. [33]). Therefore, we used simple gradient relations for the turbulent stresses and fluxes which kept tensor invariance in density variable flows (Jones [31]):

$$-\left\langle u_i^{"} u_j^{"} \right\rangle = \nu_t \left(\frac{\partial \langle u_i \rangle}{\partial x_j} + \frac{\partial \langle u_j \rangle}{\partial x_i} \right) - \frac{2}{3}\delta_{ij}\left(k + \nu_t \frac{\partial \langle u_\alpha \rangle}{\partial x_\alpha} \right), \tag{6}$$

$$-\left\langle u_i^{"} \varphi^{"} \right\rangle = \frac{\nu_t}{\sigma_\varphi} \frac{\partial \langle \varphi \rangle}{\partial x_i}, \tag{7}$$

$$\nu_t = C_\mu k^2 / \varepsilon, \tag{8}$$

where ν_T is eddy viscosity, φ is scalar variable, k is the turbulent kinetic energy (TKE), ε is the dissipation rate of TKE, σ_φ is the turbulent Prandtl number, C_μ is constant.

We used an auxiliary function $\Phi = P/\rho$ in order to derive equation (3) for pressure from the equation of transport of internal energy with Favre-Reynolds averaging. For the ideal gas, this function depends only on the temperature and concentration of gas. This makes possible to use gradient relations (7) also for the parameterization of the turbulent flux $\left\langle u_i^{"}\Phi^{"}\right\rangle$ in equation (3). The transport equations of the $k-\varepsilon$ model for the flows with density variations are given by

$$\frac{\partial\overline{\rho}k}{\partial t}+\frac{\partial\overline{\rho}u_\alpha k}{\partial x_\alpha}-\frac{\partial}{\partial x_\alpha}\frac{\overline{\rho}\nu_t}{\sigma_k}\frac{\partial k}{\partial x_\alpha}=\overline{\rho}G_T-\overline{\rho}\varepsilon\,, \tag{9}$$

$$\frac{\partial\overline{\rho}\varepsilon}{\partial t}+\frac{\partial\overline{\rho}\left\langle u_\alpha\right\rangle\varepsilon}{\partial x_\alpha}-\frac{\partial}{\partial x_\alpha}\frac{\overline{\rho}\nu_t}{\sigma_\varepsilon}\frac{\partial\varepsilon}{\partial x_\alpha}=\frac{\overline{\rho}\varepsilon}{k}\left(C_{1\varepsilon}G_T-C_{2\varepsilon}\varepsilon\right), \tag{10}$$

where $G_T=-\left\langle u_i^{"}u_j^{"}\right\rangle\partial\left\langle u_i\right\rangle/\partial x_j+\left(1/\overline{\rho}^2\right)\overline{u_i^{"}\rho^{'}}\left(\partial\overline{P}/\partial x_i\right)=s+b$ describes TKE generation due to interaction of the Reynolds stresses with gradients of the mean velocity (*s*) and generation or suppression of turbulence due to interaction of the density flux with the gradient of the mean pressure (*b*). In the Boussinesq approximation, *b* coincides with the traditional expression for the work of the buoyancy forces on the turbulent displacement of gas. The turbulent flux of the density is also calculated using the gradient formula (Jones [31], Sarkar and Lakshmanan [32])

$$\overline{u_i^{"}\rho^{'}}=-\frac{\nu_t}{\sigma_\rho}\frac{\partial\overline{\rho}}{\partial x_i}. \tag{11}$$

The turbulent Prandtl number σ_φ, following to Chan [18], was defined from the relationship Ueda et al. [34]: $\sigma_\varphi=\sigma_0\left(1-\mathrm{Rf}\right)^2/\left(1-10\,\mathrm{Rf}\right)$ for all scalars. Here, the flux Richardson number $\mathrm{Rf}=b/s$, and constant $\sigma_0=1.015$. The values of the constants of the turbulence model are standard: $C_\mu=0.09$, $C_{1\varepsilon}=1.44$, $C_{2\varepsilon}=1.92$.

2.2 Boundary and initial conditions

Let us consider boundary and initial conditions of the system of equations (1)-(5), supplemented with the turbulence model (6)-(10). Near the Earth's surface $z = 0$ below the first computational level $z < z_1$, all variables were assumed to satisfy the relationships of the Monin-Obukhov similarity theory (MOST). The MOST was developed for a stationary and horizontally homogeneous surface layer (Monin and Yaglom [35]). Applicability of the MOST-based boundary conditions is limited to the small ratio of characteristic time of turbulence to the characteristic time of significant changes of averaged variables and conditions of smooth terrain. There is no universal theory for the cases in which these conditions are not fulfilled, but for engineering applications MOST is usually considered suitable (Bartzis *et al*. [16]).

In the present studies, at the first computational level, the turbulent fluxes through the bottom surfaces of the computational cells adjacent to the bottom surface of the computational domain of all variables were calculated according to MOST. For the velocities it resulted in:

$$w_{z=z_1/2} = 0,\ \nu_T \left.\frac{du}{dz}\right|_{z=z_1/2} = u_*^2 \frac{u(z_1)}{U(z_1)},\ \nu_T \left.\frac{dv}{dz}\right|_{z=z_1/2} = u_*^2 \frac{v(z_1)}{U(z_1)}, \qquad (12)$$

where $U = U(z_1)$ is the absolute value of the horizontal component of velocity at the first computational layer, $u_* = \sqrt{-\langle u'w' \rangle}$ is the friction velocity, defined either for neutral conditions

$$u_* = \frac{\kappa U}{\ln(z_1 / z_0)} \qquad (13)$$

or from the general MOST relations, as described below. Here $\kappa = 0.39$ is von Karman constant .

The absence of the gas flow through the solid boundary was assumed everywhere except for the source of gas:

$$\frac{\nu_T}{\sigma_C}\frac{\partial\langle C\rangle}{\partial z}\bigg|_{z=z_1/2}=0. \tag{14}$$

The heat exchange with the underlying surface is described by the boundary condition:

$$\frac{\nu_T}{\sigma_T}\frac{\partial\langle T\rangle}{\partial z}\bigg|_{z=z_1/2}=-\langle T'w'\rangle_s=-q_s. \tag{15}$$

Here, T_s is the temperature of the underlying surface, and q_s is the turbulent flux of temperature through the surface. The methods of calculating q_s are given in the next section. From (15), together with (14) and (5), it follows:

$$\frac{\nu_T}{\sigma_T}\frac{\partial\bar{\Phi}}{\partial z}\bigg|_{z=z_1/2}=-\frac{q_s}{\left(R_a(1-\langle C\rangle)+R_g\langle C\rangle\right)}, \tag{16}$$

where the value of $\langle C\rangle$ is taken at $z=z_1$.

Boundary conditions for the turbulent kinetic energy and dissipation rate were defined from the assumption of the local equilibrium of the developed turbulence near the Earth's surface i.e. $b+s=\varepsilon$. For $z<z_1$ this relation is approximately

$$u_*^2\frac{dU(z)}{dz}+\frac{g}{\bar{\rho}(z)}\overline{w''\rho'}=\varepsilon(z)=\frac{C_d\left[k(z)\right]^{3/2}}{\kappa z}, \tag{17}$$

where C_d is constant. When the heat flux through the Earth's surface was absent, it was assumed that the first term in (17) dominates in the generation of the TKE near the surface and the suppression of turbulence by the stable stratification was not taken into account. In this case, from (17) and from the relationships for the turbulent logarithmic layer over the horizontal surface we obtained

$$k\big|_{z<z_1}=u_*^2/C_\mu^{1/2},\ \varepsilon\big|_{z<z_1}=u_*^3/\kappa z. \tag{18}$$

The combination of (18) and (8) yields $C_d = C_\mu^{3/4}$.

In the case of the heat exchange of the cold gas with the surface:

$$\left.\frac{dU}{dz}\right|_{z<z_1} = \frac{u_*}{\kappa z}\varphi_m(\varsigma),$$
$$\left.\frac{dT}{dz}\right|_{z<z_1} = -\frac{q_s}{u_*\kappa z}\varphi_T(\varsigma), \tag{19}$$

where $\zeta = -z/L$, $L = -u_*^3/(\kappa\beta q_s)$ is the Monin-Obukhov length scale, $\beta = g/T_s$ is the buoyancy parameter, and φ_m, φ_T are the so-called stability functions (Monin and Yaglom, [35]). A general form of the functions φ_m, φ_T covering all ranges of positive values of $\zeta = -z/L$ is unknown. However, in Kader and Yaglom [36], three asymptotic forms of these functions were established, based on similarity considerations and experimental data. Brutsaert [38] proposed interpolation formulas for φ_m, φ_T which were based on these functions:

$$\varphi_m(\varsigma) = \frac{a + b\varsigma^{m+1/3}}{a + \varsigma^m},\ a = 0.33, b = 0.41,\ m = 1;$$
$$\varphi_T(y) = \frac{c + d\varsigma^n}{c + \varsigma^n},\ c = 0.33, d = 0.057,\ n = 0.78. \tag{20}$$

Differentiating (17) by z, using (19) and assuming that $\nu_T\big|_{z<z_1} = C_\mu^{1/4}\sqrt{k}\kappa z$ we found boundary conditions for k and ε:

$$\nu_T \left.\frac{\partial\varepsilon}{\partial z}\right|_{z=z_1/2} = -\frac{u_*^4}{z} + \frac{u_*^4}{L}\frac{\varphi_m'(\varsigma)}{\varphi_m(\varsigma)} + \frac{q_s^2}{T^2}\frac{g\varphi_T(\varsigma)}{\varphi_m(\varsigma)},$$
$$\nu_T \left.\frac{\partial k}{\partial z}\right|_{z=z_1/2} = \left(\frac{2C_\mu^1\kappa z}{3}\right)\left(\frac{\kappa g q_s}{T} + \frac{u_*^3}{C_d L}\varphi_m'(\varsigma)\right). \tag{21}$$

Under neutral stratification ($q_s = 0,\ \varphi_m = \varphi_T = 1$) the relations (21) reduced to equivalent boundary conditions (22):

$$\nu_T \left.\frac{\partial k}{\partial z}\right|_{z=z_1/2} = 0,\ \nu_T \left.\frac{\partial \varepsilon}{\partial z}\right|_{z=z_1/2} = -\frac{u_*^4}{z}. \qquad (23)$$

In order to determine the value of the temperature of the surface T_s, the coupled problem of the heat transfer in the surface layer of the Earth was solved because the heat transfer in the Earth can significantly influence the dynamics of the cold of gas cloud (Nielsen and Ott [2]). The heat transfer in the Earth surface layer was calculated with the use of the equation of heat conduction in the soil:

$$\rho_s c_{ps} \frac{\partial T}{\partial t} = \chi \frac{\partial^2 T}{\partial z^2}\ , \qquad (24),$$

where ρ_s and c_{ps} are the density and specific heat capacity of the soil, respectively, χ is the heat conductivity of the soil and axis z is directed downward. The initial temperature distribution in the soil was taken to be constant: $T(z,0) = T_{0s}$. The boundary conditions are

$$\rho_s c_s \chi \left.\frac{\partial T}{\partial z}\right|_{z=0} = \left\langle T'w' \right\rangle_s ;\ T\big|_{z=H} = T_\infty = T_{0s}\,, \qquad (25)$$

where T_∞ is undisturbed soil temperature at large depth.

On the upper boundary of the computational domain, distributions of all variables correspond to the atmospheric conditions undisturbed by the gas release. Turbulent characteristics in the surface layer of the atmosphere can be determined from the MOST. The computational domain was oriented in the direction of the main wind vector near the surface. On the lateral boundaries, where the flow approached the domain, undisturbed distributions of all variables were used as boundary conditions. On the other lateral boundaries, the condition $\partial\varphi/\partial\mathbf{n} = 0$ for all variables was used, where **n** is the normal vector to the lateral boundary. The initial undisturbed conditions for all meteorological parameters were calculated from the MOST theory.

2.3 Parameterization of the heat exchange with the surface

A. Parameterization using the relationships for the forced convection

In this approach, the heat flux from the surface was represented as:

$$\left\langle w'T' \right\rangle = \lambda \left(T_s - T\left(z_1\right) \right), \tag{26}$$

where the heat transfer coefficient λ was defined by equations of Yaglom and Kader [37] for the forced convection:

$$\lambda = \frac{u_*}{\left(2.12\ln(z/h) + h_+^{1/2} 0.55(\mathrm{Pr}^{2/3} - 0.2) + 9.5\right)}, \tag{27}$$

where h is the average height of the roughness elements, which is related to the roughness height as $h \approx 30 z_0$ (Monin and Yaglom [35]), $h_+ = h u_* / \nu$, ν and Pr are molecular viscosity and the Prandtl number, respectively. The friction velocity was determined from (13).

B. Parameterization using interpolation formula for the heat transfer coefficient

In this approach, the heat flux from the surface was also represented with the help of (26). However, the heat transfer coefficient was calculated using simple interpolation formula:

$$\lambda = \lambda_1 + \lambda_2 = \lambda_1 + C_0 \left(\left(T_S - \left\langle T \right\rangle \right) \left(\beta \nu / \mathrm{Pr} \right) \right)^{1/3}, \tag{28}$$

which accounted for both forced and free convection asymptotic regimes. Here, λ_1 was defined by (27), λ_2 accounted for the free turbulent convection (Zilitinkevich [39]) and $\beta = g / T_s$. The value of constant C_0 was obtained by different authors in the range of 0.1-0.21 (Zilitinkevich [39]). In this study, $C_0 = 0.21$ was adopted. The friction velocity was determined from (13).

C. Parameterization using similarity relationships for mixed convection

In this approach, vertical profiles of temperature and wind velocity near the wall are represented in the similarity form (Monin and Yaglom [35]):

$$U(z_1)=\frac{u_*}{\kappa}\left[\ln\left(\frac{z_1}{z_0}\right)-\Psi_m\left(\frac{z_1}{L}\right)+\Psi_m\left(\frac{z_0}{L}\right)\right],$$
$$T_s-T(z_1)=\frac{\left\langle w'T'\right\rangle}{\kappa u_*}\left[\ln\left(\frac{z_1}{z_{0T}}\right)-\Psi_T\left(\frac{z_1}{L}\right)+\Psi_T\left(\frac{z_{0T}}{L}\right)\right], \tag{29}$$

where z_0, z_T are roughness lengths for momentum and temperature. Functions Ψ_m, Ψ_T are defined as:

$$\Psi_{m,T}\left(z_1/L\right)=\int_0^{z_1/L}\frac{1-\varphi_{m,T}(\varsigma)}{\varsigma}d\varsigma\,. \tag{30}$$

Substituting (20) into (30) and calculating resulting integrals analytically, Brutsaert [38] obtained functions Ψ_m, Ψ_T as

$$\Psi_m(y)=\ln(a+y)-3by^{1/3}+0.5ba^{1/3}\ln(\frac{(1+x)^2}{1-x+x^2})+$$
$$\sqrt{3}ba^{1/3}\arctan\left[(2x-1)/\sqrt{3}\right]+\text{const},$$
$$\Psi_T(y)=\left[(1-d)/n\right]\ln\left[(c+y^n)/c\right], \tag{31}$$
$$x=\left(\frac{y}{a}\right)^{1/3},\ y=-z_1/L.$$

The temperature roughness length z_{0T} was determined in Yaglom and Kader [37] as

$$z_{0T}=h\exp(\left(\left(hu_*/\nu\right)^{1/2}0.55(\mathrm{Pr}^{2/3}-0.2)+9.5\right)/2.12)\,. \tag{32}$$

With given values of $T(z_1), U(z_1)$, the system of nonlinear equations (29), (31), (32) was solved by iterations for the unknown values of u_*, $\left\langle w''T''\right\rangle$, which were substituted into (21) in order to obtain boundary conditions for k and ε.

2.4 Numerical solution techniques

Numerical techniques for solving equations (1)-(4), (8)-(9) mainly follow the approach of Kovalets and Maderich [24], with modifications caused by the use of the MOST-based boundary conditions. Implicit finite-difference splitting schemes upon spatial directions and

physical processes were used (Kovenya and Yanenko [22])**.** In these splitting schemes, calculations were performed in two stages. In the first stage, the velocity components and the pressure were computed. In the second stage, other variables (density, gas concentration, turbulent kinetic energy and dissipation rate) were computed. This approach allowed for high accuracy mass conservation and an increased stability of the scheme. The finite-volume method (Patankar [21]) was used in order to discretize the governing equations. The scheme described by Patankar [21] was applied to the finite-difference approximation of the operators of convection-diffusion.

3. Results

3.1 Simulation of the laboratory experiment with continuous isothermal release (Zhu *et al.* [4])

In order to study interaction of an atmospheric surface layer with an almost isothermal heavy gas cloud, we reproduced numerically conditions of laboratory experiments by Zhu *et al*. [4]. Those experiments were conducted in the wind tunnel with height 2.1 m, width 3.7 m. and length 18.3 m. An aerodynamically rough surface was created with the use of the roughness elements (plates with height h_0=25 mm and width 5 cm). In the experiments, the stationary flow of carbon dioxide (CO_2) from a source located at the bottom of the wind tunnel into the boundary layer was studied. The source was located at a distance of 8.95 m from the beginning of the tunnel. The density of the CO_2 under the atmospheric pressure was $\rho_{g0} = 1.72\rho_a$. Before the beginning of the release, a neutral zero-pressure boundary layer was established. The height of the boundary layer in the tunnel δ_r was approximately 1m. The velocity U_r of the flow at the height δ_r in experiments was 0.5, 0.75, 1.0 and 2.0 m/s. Correspondingly, the Reynolds number varied from $3 \cdot 10^4$ to 10^5. The roughness parameter

was $z_0 \approx 0.002$ m. The diameter of the source was $D_s = 0.104$ m and the release rate $W_s = 0.059$ m/s.

The computational domain was $8 \times 3 \times 1$ m. It was approximately equal to the size of the test section of the wind tunnel and the height of the boundary layer. The source was located at a distance $x = 1$ m from the beginning of the computational domain. The grid size in all directions was variable. Near the source, the grid size in horizontal directions was the smallest: $\Delta x = \Delta y = 0.1$ m. The grid size in vertical direction Δz was the smallest near the surface: $\Delta z = 0.001$ m. The calculations were performed in two stages. In the first stage, an undisturbed boundary layer was calculated in order to reproduce measured stationary profiles of mean velocity and TKE. In the second stage, the undisturbed fields of velocity, TKE and dissipation rate were used as initial conditions and the upstream boundary condition.

The effect of buoyancy forces on the distribution of the ground-level concentration is shown in Figure 1 where calculated distributions of concentration for neutrally buoyant and heavy gases are shown. The heavy gas cloud covers a much larger area than the neutral gas cloud does. The same pattern was observed in experiments with the hydraulic flume (Britter **[**40**])** where salt water from a source flew into a flow of fresh water. Figure 2 shows experimental and calculated distributions of the height of the cloud L_V along the axis of symmetry of the wind tunnel for different wind velocities. The value of L_V both in experiments and calculations was defined as the height where concentration is reduced to 10% of the ground level value. The calculated height of the cloud changes slowly initially due to the damping of the turbulence by the stable stratification in the gas cloud. However, it increases subsequently due to the turbulent entrainment. Britter [40] estimated the lateral length scale L_H and vertical scale L_V of a heavy gas plume assuming the superposition of buoyancy driven lateral spread and longitudinal advection by wind without mixing. The

asymptotic values of height $L_V^{'}(x)$ and width $L_H^{'}(x)$ of plume at a distance from the heavy gas source $x >> D_S$ are

$$\frac{L_V'}{L_B} = \frac{1}{2C_B}\left(\frac{q_0}{U_{\mathrm{r}}}\right) L_B^{-1/3} x^{-2/3}, \qquad \frac{L_H'}{L_B} = 2C_B\left(\frac{x}{L_B}\right)^{2/3}, \tag{33}$$

where $L_B = g_0' q_0 / U_{\mathrm{r}}^3$ is the buoyancy length scale, $g_0' = (\rho_{g0} - \rho_a)/\rho_a$ is the initial buoyancy, q_0 is the volume flux in the source, $C_B \approx 0.25$ is an empirical constant. However, dependence (33) for $L_V^{'}$ does not agree with experiments and simulations in Figure 2, where an increase of the cloud height due to mixing is observed, in contrast to the collapse of the cloud predicted by (33). At the same time, simulated dependences of L_H (curves 2 and 3 in Figure 3a) approach the analytical dependence (33) (curve 1). It implies that the lateral gravitational spread of the heavy gas cloud is much larger than the horizontal turbulent diffusion. The velocity of the gravitational lateral spread is $V \sim (g'(x) L_V(x))^{1/2}$. Hence, the reduction of buoyancy $g'(x) = g(\rho(x) - \rho_a)/\rho_a$ caused by mixing of the cloud with the ambient air should be compensated by an increase of the height of the cloud L_V in order to agree with dependence (33) for L_H (Britter [40]). Consequently, the relationship $L_H' \sim L_H$ occurs when similarity relationship $\Pi_1 \sim \Pi_2$ holds, where $\Pi_1 = \sqrt{L_V'(x)/L_V(x)}$ and $\Pi_2 = \sqrt{g^{'}(x)/g_0^{'}}$. The results of the calculations in Figure 3b confirm this similarity for large distances from the source, i.e. for small values of $g^{'}(x)$ and Π_1.

The buoyancy forces suppress turbulent mixing, but at the same time the larger surface area of the plume enhances the entrained volume of the ambient air. Therefore, the resultant distribution of the ground-level concentration at the axis of symmetry of the cloud $\langle C(x,0,0)\rangle$ depends weakly on the buoyancy g_0' in the source (Britter [1]). Neff and

Meroney [41], on the basis of laboratory experiments with continuous isothermal release of a heavy gas on an aerodynamically smooth surface, established an empirical scaling for the ground level concentration at a downwind distance x as $\langle C(x,0,0)\rangle / C_0 = \Psi\left(xU_r / \left(q^{3/5} g_0'^{1/5}\right)\right)$. As seen in Figure 4, both the measured (Zhu *et al*. [4]) and simulated volume concentration distributions $\langle C_{vol}(x,0,0)\rangle$ also agree with this scaling for a rough surface. The ground-level concentration at a large distance decays slightly slower than the asymptotics $\langle C_{vol}(x)\rangle \sim x^{-5/3}$ for neutrally buoyant gas (Monin and Yaglom [35]). The spikes in the experimental data at small distances from the source were caused by individual roughness elements.

The vertical profiles of the mean velocity and concentration of gas, TKE and the Richardson number $\mathrm{Ri}=-(\mathrm{g}/\overline{\rho}_{\mathrm{a}})(\partial\overline{\rho}/\partial z)/\left(\partial\langle u\rangle/\partial z\right)^2$ are shown in Figure 5. The vertical turbulence intensity $\sqrt{\overline{w'^2}}$ measured by Zhu *et al*. [4] and the calculated values of $\sqrt{(2k/3)}$ in Figure 5 (c) are normalized on the local velocities of the flow $\overline{u}(z)$. The experimental and calculated profiles in Figure 5 agree well. As is seen from the figure, the $k-\varepsilon$ turbulence model predicts suppression of the turbulence due to the stable stratification in the cloud in accordance with the experiment. This effect is maximum in the upper part of the cloud where the density gradient is the largest. The profiles of the Richardson number in Figure 5 (d) have maximum coinciding with the level where stratification is the largest. The calculated vertical profiles of the turbulent shear stress $-\langle u''w''\rangle = \nu_t \partial\langle u\rangle/\partial z$ at different distances from the source are presented in Figure 6. The damping of the turbulence by the stratification and diminishing of the velocity shear at the upper boundary of the cloud result in a characteristic minimum of the shear stress. The height of this minimum is proportional to L_V (Figure 2). The maximum calculated reduction of the turbulent shear stress at the top of the cloud was

five times the undisturbed value. The suppression of the turbulence due to the stratification resulted in reduction in the drag forces and thus acceleration of the mean velocity in the boundary layer above the top of the cloud compared with the undisturbed boundary layer. This effect is observed both in experiments and in the simulations shown in Figure 5 (a) and (b). The calculated maximum increase of the mean velocity due to this effect was 1.3 of the undisturbed value. The vertical profile of the neutrally buoyant gas concentration was close to the Gaussian, while the vertical profile of the heavy gas could be approximated by an exponent (Zhu *et al*. [4]). For sufficiently large Richardson numbers, the entrainment of the air through the upper boundary of the cloud was suppressed near the source, as can be seen in Figure 2 (curve 1) which describes dependence of the cloud's height on the distance from the source.

The calculated surface friction velocity $u_* = -\left\langle u'' w'' \right\rangle\Big|_{z=z_1}$ also decreased near the source as is shown in Figure 6. It is explained by the fact that a heavy gas, covering the roughness elements, serves as a new underlying surface for the ambient flow of the air. The calculations showed that the corresponding displacement height $\delta_u = \int_{z_0}^{\delta_r} \left[\left(\langle u \rangle - \langle u_a \rangle \right) / U_r \right] dz$ was near 10-12 mm which was comparable with the height of the roughness elements. Here $\langle u_a \rangle$ is the velocity of the undisturbed flow. The velocity in the bottom part of the heavy gas cloud was reduced in comparison with the undisturbed flow (Figure 5 a) as a result of the displacement of the boundary layer.

The use of the implicit finite-difference scheme allowed us to solve efficiently the unfiltered equations of compressible flow at a low Mach number. Lets us consider now the role of density variations in the flow dynamics. The parameter $\beta = \max_{i,j,z} \left(\left| \frac{1}{\rho} \frac{d\rho}{dt} \right| / \left(\max_k \left(\left| \frac{\partial u_k}{\partial x_k} \right| \right) \right) \right)$ is the maximum of the ratio of the term $\left| (1/\rho)(d\rho/dt) \right|$

to the largest by absolute value component of the divergence term $\partial u_k / \partial x_k$ in the same point of the computational domain. The maximum value of the parameter is $\beta = 3$. It is achieved when all three components $\partial u_k / \partial x_k$ are equal. This parameter characterizes the error introduced into the continuity equation by the Boussinesq approximation. Variation of β with distance from source for $U_r = 0.5\,\text{m/s}$ is shown in Figure 7. The parameter β achieved its maximum value $\beta = 2$ at a distance 1 m, falling to the values less than 0.1 after 2 m downwind. It is important that most changes in the structure of turbulence in this experiment took place in the first 2 m downwind from the dense gas source, where the Boussinesq approximation is not valid and where compressibility should be taken into account in the continuity equation.

3.2 Simulation of the field experiment with a cold gas release (Koopman et. al., [27])

A study of a cold heavy gas dispersion in the atmosphere was carried out using the conditions of field experiment BURRO 8 in which the dispersion of liquefied natural gas (LNG) was studied (Koopman *et al*. [27]). The Burro Series of LNG spill experiments was performed at the Naval Weapons Center, China Lake, California. In experiment BURRO 8, approximately 40 m^3 of LNG was poured into a circular water basin at spill rate of approximately 117 kg/s. The diameter of the basin was 58 m. The measurements of concentration were conducted at radii of 57, 140, 400 and 800 m from the source. The wind speed was approximately 1.8 m/s and atmosphere was slightly stable (category E). The dense gas dispersion in that experiment was modeled under the assumptions of a flat terrain, a circular source with a constant diameter 58 m and a release rate 117 kg/s, lasting 107 seconds with the gas temperature $T_{exit} \approx 110°K$. The horizontal grid size near the source was approximately 17 m increasing in downwind and crosswind directions from the source and the vertical grid size was approximately 0.1 m near the ground, increasing vertically.

Simulated vertical sections of the temperature along wind at $t = 180\,s$, with and without heat exchange with the surface, in Figure 8 show that the heat exchange results in the growth of the height of the center mass of the cloud and in formation of a convective boundary layer at the bottom of the cloud. The isolines of the temperature in the cloud become closed and the cloud lifts up with distance. Therefore, the difference of temperature between cases (a) and (b) in Figure 8c is maximum near the surface, well away from the source.

Figure 9 shows the measured and simulated crosswind volume concentration distributions at a distance 140 m from the source at the time $t = 180\,s$ from the release start. Three cases of calculations are shown: (i) using relationships for the heat exchange which account for the forced convection (parameterization A), (ii) using relationships which account for the mixed convection of Brutsaert [38] (parameterization C) and (iii) using interpolation formula for the mixed convection (parameterization B). The characteristic maximum in the measured and calculated concentration distributions in Figure 9 shows the beginning of the lifting of the cloud mentioned above. The parameterization B results in a significantly higher height of the cloud (≈ 1.5 times) compared with the other parameterizations. This hight estimation is the closest to the experiment as shown in Figure 9a.

Let us estimate the difference between the experimental data and the results of the simulations. Let us define the height of the cloud H by the position of the isoline of the concentration $C = 1\%$. For the prediction of H at a given cross-section, the rms and bias errors σ_H, ε_H are, respectively:

$$\sigma_H^2 = \left(\int_{y=0}^{y=Y} \left(\left(H_m - H_{\exp} \right)^2 \Big/ \left(H_m H_{\exp} \right) \right) dy \right) / Y,$$
$$\varepsilon_H = \left(\int_{y=0}^{y=Y} \left(2\left(H_m - H_{\exp} \right) \Big/ \left(H_m + H_{\exp} \right) \right) dy \right) / Y. \qquad (34)$$

Here, $H_{\exp}$ and H_m are experimental and computed values, respectively, $Y = 100$ m is the length of the cross-section at the distance 140 m from the source (Figure 9). It was taken for positive values of y, where the terrain is flatter. For the parameterization B, $\sigma_H \approx 30\%$, $\varepsilon_H = -10\%$, while for A and C both errors were almost the same: $\sigma_H \approx 80\%$, $\varepsilon_H \approx -65\%$. The comprehensive parameterization C failed to bring an improvement of the results of the simulation and, therefore, a simple parameterization B for the mixed convection can be recommended for use in dense gas dispersion models.

In Figure 10, the maximum centerline volume concentrations observed in BURRO 8 experiment are shown together with the predictions of the model at the height 1 m, where gas sensors were placed. Four variants of the predictions are given to show the role of different parameterizations of the heat exchange. In the worst case, the heat exchange is not taken into account at all. It results in underestimation of the maximum concentration close to the source by a factor of 1/4, because a relatively small height of the cloud was predicted at the sensor level. Far from the source, the values of concentration were overestimated, because the dilution was reduced by the stable stratification in the cloud. When the heat exchange was parameterized with the relationships which accounted for the forced convection (parameterization A), the agreement was good in the region far from the source. However, near the source, where velocities in the plume are relatively small, this approach also failed to predict the observed concentration. Using the parameterization C in order to account for the mixed convection did not improve the results either. The best agreement for all distances from the source was achieved using the simple interpolation formula for the heat exchange coefficient (parameterization B), when in relationship (28) both forced and free convection mechanisms were taken into account. However, in the nearest point to the source, the maximum observed concentration was underestimated by a factor of 1/2. This fact can be

explained by sensitivity of the measurements in this point to characteristics of the pool (e.g., time varying source rate).

Free convection dominates the forced convection near the cold gas source due to a large temperature difference between the gas cloud and the surface near the source. As a result, coefficient λ_2 describes the free convection. In addition, due to the reduction of the horizontal wind speed near the source, because of the vertical displacement of the boundary layer considered in Section 3.1, the heat exchange coefficient of the forced convection λ_1 decreases. This analysis is confirmed by Figure 11 which shows the spatial distributions of the heat exchange coefficients λ_1 and λ_2 in parameterization B. The reduction of λ_1 and the growth of λ_2 near the source, as well as the reduction of λ_2 and the increase of λ_1 far from the source are seen.

Let us consider now the effect of the parameterizations of the heat exchange with the Earth's surface on the cooling of the Earth's surface. The analytical solution of the heat transfer problem (24)-(26) for the heat flux $q(z,t) = \rho_s c_s \chi \partial T / \partial z$, was obtained by Nielsen and Ott [2] in the case of a constant heat transfer coefficient λ and a sudden forcing by a constant gas temperature at surface T_g. The solution for a non-dimensional heat flux at the surface describes the forced convection for a constant wind velocity:

$$\tilde{q}_1(0,t) = \exp(\tilde{t})\,\mathrm{erfc}\left(\tilde{t}^{-1/2}\right) \qquad (35),$$

where $\tilde{q}_1(0,t) = q(0,t)/q(0,0)$, $\tilde{t} = tq^2(0,0)/\left(\rho_s c_s \chi \left(T(0,t) - T_g\right)^2\right)$. The solution (35) is given in Figure 12 (solid curve). As is seen from the figure, the heat flux from the soil substantially decays with time even for a constant gas temperature. In the case of the mixed convection under constant wind velocity and constant gas temperature, the heat transfer coefficient $\lambda = \lambda_1 + \lambda_2$ defined by relationships (28) (parameterization B) consists of constant value λ_1 and variable $\lambda_2 = \lambda(\Delta T)$, which depends on the temperature difference between the gas and the Earth's surface $\Delta T = T_g - T(0,t)$. In this case, the non-dimensional heat flux through the surface is a function of two parameters:

$$\tilde{q}_{mix}(0,t) = F\left(\tilde{t}, \tilde{\lambda}\right), \qquad (36)$$

where $\tilde{\lambda} = \lambda_2(\Delta T_0)/\lambda_1$. It is obvious that: $\tilde{q}_{mix}(0,t) \xrightarrow[\tilde{\lambda}\to 0]{} \tilde{q}_1(0,t)$. In order to estimate the effect of the mixed convection on the heat flux from the soil, the problem (24)-(25), (26), (28) was solved numerically with constant gas temperature T_g and constant horizontal wind velocity. The results obtained for different values of parameter $\tilde{\lambda}$ are shown in Figure 12. As follows from the presented results, the dependence of function *F* on $\tilde{\lambda}$ is essential only for $\tilde{\lambda} < 5$, whereas for large $\tilde{\lambda}$ it tends to the free convection regime: $F(\tilde{\lambda},t) \underset{\tilde{\lambda}\to\infty}{\to} F_2(\tilde{t})$. In the case of BURRO 8 experiment, the simulated by a 3D model maximum of the reduction of the heat flux due to the cooling of the Earth's surface was $\tilde{q}_1 \approx 0.95$ in parameterization A and $\tilde{q}_{mix} \approx 0.83$ in parameterization B. Therefore, the relative contribution of the mixed convection to the cooling of the Earth's surface in BURRO 8 experiment was $(\tilde{q}_2 - \tilde{q}_1)/\tilde{q}_1 \approx 13\%$.

CONCLUSIONS

The presented paper improves the numerical three-dimensional model of a heavy gas dispersion in an atmospheric surface layer developed earlier by Kovalets and Maderich [24]. It also presents the results of a numerical simulation of the interaction of a heavy gas cloud with an atmospheric surface layer. The model used is based on the unfiltered system of gas-dynamic equations which allow for reproducing the dynamics of a heavy gas cloud both near the source, where the effects of density variations are essential, and far from the source, where the Boussinesq approximation is valid. The system of model equations was used in a form of equations for density-velocity-pressure-concentration. This has essential numerical advantages in the case of the ideal gas law. The turbulence was parameterized using the *k*-ε model. Three parameterizations of the heat exchange with the Earth's surface were considered: (A) formula of Yaglom and Kader [37] for the forced convection, (B) interpolation formula for the mixed convection and (C) approach of Brutsaert [38] based on a scaling relationships of Kader and Yaglom [36]. The problem of the cold gas dispersion was

coupled with the problem of the heat transfer in the surface layer of the Earth. This model is intended mainly for basic studies.

Two case studies were considered. In the first study based on experiment of Zhu *et al*. [4], interaction of an isothermal heavy gas plume with an atmospheric surface layer was simulated. It was shown that stable stratification in the cloud essentially suppresses the turbulence in the plume, reducing the turbulent momentum flux by a factor of down to 1/5 in comparison with the undisturbed values. This reduction substantially influences velocities in the atmospheric boundary layer above the cloud, increasing the mean velocity by a factor of up to 1.3 in comparison with the undisturbed values. The turbulent shear stress at the surface is also diminished in the region close enough to the source due to the displacement of the atmospheric boundary layer by the heavy gas. The characteristics of the atmospheric boundary layer in the presence of a heavy gas cloud and concentration distributions calculated with the use of the simple isotropic k-ε turbulence model agree well with the observations in experiments of Zhu *et al*. [4]. This agreement can be explained by the fact that the lateral spreading of the plume is dominated by the buoyancy forces, whereas the turbulent diffusion significantly influences only the vertical spreading.

In the second case study, simulation of a cold heavy gas dispersion and comparison with field experiment BURRO 8 showed significant influence of both forced and free convection components of the mixed convection under the moderate wind speeds. Three cases were studied: (i) using relationships of Yaglom and Kader [37] for the heat exchange which accounted for the forced convection (parameterization A), (ii) using interpolation formula for the mixed convection (parameterization B) and (iii) using relationships of Brutsaert [38] which accounted for the mixed convection of (parameterization C). It was shown that parameterization B for the mixed convection significantly improved results of simulation in comparison with the calculations with the forced convection only. The comprehensive

parameterization C, however, failed to bring a significant improvement of the results of the simulation. This fact can be considered a general failure of MOST to describe adequately the nearly shear–free convective boundary layer, due to the existence of large-scale coherent structures (buoyancy driven convective cells) which are neglected by MOST (see Zilitinkevich *et al*. [41]). It is therefore advised to use the simple parameterization B in dense gas dispersion models. The free convection mostly affects the cold dense gas dispersion sufficiently close to the source where temperature differences are large and the forced convection is damped due to the effect of the boundary layer displacement as discussed in Section 3.1.

ACKNOWLEDGEMENTS

This work has been partly supported by the National Scholarship Programme of the World Federation of Scientists. This article benefited from comments and suggestions of two anonymous reviewers. The authors also thank Oleksiy Danylenko for his valuable comments and suggestions.

REFERENCES

1. Britter R. E.: 1989, Atmospheric dispersion of dense gases, *Ann. Rev. Fluid Mech*., **21**, 317-344.
2. Nielsen M. and Ott S.: 1999, Heat transfer in large-scale heavy-gas dispersion, *J. Hazard. Materials*, **67,** 41-58.
3. Meroney R.N. and Neff D.E.: 1986, Heat transfer effects during cold dense gas dispersion: Wind tunnel simulation of cold gas spills. *Trans. ASME J. Heat Transfer*, **108**, 9-15.

4. Zhu G., Arya P. and Snyder.: 1998, An experimental study of the flow structure within a dense gas plume, *J. Hazard. Materials*, **62**, 161-186.
5. Ding J., Arya S.P. and Snyder W.H.: 2001, Experimental study of the criteria of flow laminarization in two-dimensional dense gas plumes, *Env. Fluid Mechanics*, **1**, 281-309.
6. Briggs G.A., Britter R.E., Hanna S.R., Havens J.A., Robins A.G. and Snyder W.H.: 2001, Dense gas vertical diffusion over rough surfaces: results of wind-tunnel studies. *Atmos. Environ.*, **35**, 2265-2284.
7. Meroney R.N.: 1987, Guidelines for fluid modeling of dense gas cloud dispersion, *J. Hazard. Mater.*, **17**, 23-46.
8. Koopman R. P., Ermak D. I. and Chan S. T.: 1989, A review of recent field tests and mathematical modelling of atmospheric dispersion of large spills of denser-than-air gases, *Atmos. Environ.*, **23**, 731-756.
9. Hanna S.R., Drivas P.J. and Chang J.C.: 1996, *Guidelines for use of vapor cloud dispersion models*, 2nd ed. CCPS. A.I.Ch.E., NY, 271 pp.
10. Evans K.: 1993, ALOHA and ARCHIE: a comparison, Report No HAZMAT 93-2, NOAA, Seattle, Washington.
11. Witlox, H.W.M., 1994. The HEGADAS model for ground-level heavy-gas dispersion } II. Time dependent model. *Atmos. Environ*. **28**, 2933-2940.
12. Sykes R.I., Cerasoli C.P., Henn D.S.: 1999, The representation of dynamic flow effects in a Lagrangian puff dispersion model, *J. Hazard. Mater.*, **A64**, pp.223-247
13. Hankin R.K.S., Britter, R.E.: 1999, TWODEE: the Health and Safety Laboratory's shallow layer model for dense gas dispersion. Part I. Mathematical basis and physical assumptions, *J. Hazard. Mater*. **66**, 211–226.

14. Venetsanos A.G., Bartzis J.G., Wurtz J., Papaliou D.D.: 2003, DISPLAY-2: a two-dimensional shallow layer model for dense gas dispersion including complex features, *J. Hazard. Mater.,* **99**, pp. 111-114.
15. Edigarov A. C.: 1990, Numerical calculation of the turbulent flow of the cold heavy gas cloud in the atmosphere, *J. Num. Math. and Math. Phys.*, **31**, 1369-1380.
16. Bartzis J.G., N. Catsaros, M. Varvayanni, A. Venetsanos, S. Andronopoulos, D. Vlachogianiss, K. Konte, 1995, ADREA-HF: A three dimensional finite volume code for vapour cloud dispersion in complex terrain. Model description and users' manual, DEMO report, NCSR "DEMOKRITOS", Greece.
17. Pereira J.C.F., Chen X.Q., 1996, Numerical calculations of unsteady heavy gas dispersion. *J. Hazard. Mater.*, **46**, 253-272.
18. Chan S.T.: 1997, A three-dimensional model for simulating atmospheric dispersion of heavy-gases over complex terrain. *Preprint UCRL-JC-127475*, LLNL, Livermore, USA, 7 p.
19. Konig-Langlo G., Schatzmann M.: 1991, Wind tunnel modeling of heavy gas dispersion, *Atmos. Environ.*, **25A** , pp. 1189-1198.
20. Nettervile D.G.: 1989, Plume rise, entrainment and dispersion in ambient winds, *Atmos. Environ.*, **15**, pp. 1061-1081.
21. Patankar S.V.: 1980, *Numerical heat transfer and fluid flow*, Hemisphere Publishing Corporation.
22. Kovenya V.M. and Yanenko N.N.: 1981, *Splitting method in the problems of the gas dynamics*, Nauka Publishers, Novosibirsk .
23. Kovalets I.V. and Maderich V.S.: 1999, Dynamics and energetics of the heavy gas dispersion in the surface layer of the atmosphere, *Prykladna Hydromekhanika* (*Applied*

Hydromechanics), **1(73)**, No 4, 11-18. (English translation in *International Journal of Fluid Mechanics Research* , 2003, **30**, №4, 410-424.)

24. Kovalets I.V. and Maderich V.S.: 2001, Numerical 3D model of the heavy gas dispersion in the atmosphere with the use of the conservative splitting schemes, *Prykladna Hydromekhanika* (*Applied Hydromechanics*), **3(75)**, №1, 28-36. (English translation in *International Journal of Fluid Mechanics Research* , 2003, **30**, №4, 410-424.)
25. McQuaid J., Roebuck B.: 1984, Large scale field trials on dense vapour dispersion. Final Report to Sponsors on the Heavy Gas Dispersion Trials, Thorney Island 1982-84, HSE 1984.
26. Western Research Institute (WRI), 1998. Final Report on the 1995 Kit Fox project, WRI, Laramie, Wyoming.
27. Koopman R.P., Baker J., Cederwall R. T., Coldwire H.C., Hogan W. J., Kamppinen L. J., Kiefer R. D., McClure J. D., McRae T. G., Morgan D. L., Morris L. K., Span M. W.: 1982, *BURRO series data report LLNL/NWC 1980 LNG spill tests*, report UCID-19075, LLNL.
28. Goldwire H.C., et. al., 1983, COYOTE series data report LLNL/NWC 1981 LNG spill tests dispersion, vapor burn, and rapid phase transition, UCID-19953, Vol. 1, LLNL.
29. Hanna S.R., Strimaitis D.G., Chang J.C.: 1991, Evaluation of fourteen hazardous gas models with ammonia and hydrogen fluoride data, J. Hazard. Mater., 26/2, pp. 127-158
30. Favre A.: 1969, Statistical equations of turbulent gases. In: *Problems of Hydrodynamics and Continuum Mechanics*, SIAM, Philadelphia, 37-44.
31. Jones W.P.: 1980, Models of the turbulent flows with variable density and combustion, In: *Kollmann (ed.), Prediction methods for turbulent flows*, Hemisphere, 349-398.
32. Sarkar S. and Lakshmanan B. : 1991, Application of a Reynolds stress turbulence model to the compressible shear layer, *AIAA J.*, **29**, 743-749.

33. Adumitroaie V., Ristorchelli R.J. and Taulbee D.B.: 1999, Progress in Favre-Reynolds stress closures for compressible flows, *Phys. Fluids*, **11**, 2696-2719.
34. Ueda H.S., Mitsumoto S. and Komori S.: 1981, Buoyancy effects on the turbulent transport processes in the lower atmosphere. *Quart. J. R. Met. Soc.,* **107**, 561-578.
35. Monin A.S., Yaglom A.M.: 1971, *Statistical fluid mechanics:Mechanics of turbulence*. V.1. MIT Press, Cambridge Mass.
36. Kader B.A., Yaglom A.M.: 1990, Mean fields and fluctuations moments in unstably stratified turbulent boundary layers, *Journal of Fluid Mechanics*, **212**, 637-662.
37. Yaglom A.M., Kader B.A.: 1974, Heat and mass transfer between rough wall and turbulent fluid flow at high Reynolds and Peclet numbers, *Journal of Fluid Mechanics*, **62**, 601-623.
38. Brutsaert W.: 1999, Aspects of bulk atmospheric boundary layer similarity under free convective conditions, *Reviews of Geophysics*, **37**, 439-451
39. Zilitinkevich, S. S.: 1991, *Turbulent Penetrative Convection*. Avebury Technical, Aldershot.
40. Britter R.: 1980, The ground level extent of a negatively buoyant plume in a turbulent boundary layer, *Atmos. Environ.*, **14,** 779-785.
41. Neff D.E., Meroney R.N.: 1982, The behaviour of LNG vapor clouds: wind tunnel tests on the modeling of heavy plume dispersiuon, Final Report, CER81-82DEN-RNM25, Gas Research Institute, Chicago, Illinois.
42. Zilitinkevich S., Grachev A., Hunt J.C.R.: 1998, Surface frictional processes and non-local heat/mass transfer in the shear-free convective boundary layer, *Buoyant Convection in Geophysical Flows*, (E. J. Plate et. al., eds.), 83, 113, Kluwer Academic Publishers.

CAPTIONS

Figure 1 Calculated ground-level concentration of heavy gas (a) and neutrally buoyant gas (b) with wind velocity at 1m height $U_r = 0.5$ m/s. The isolines correspond to the values of concentration: 0.005, 0.01, 0.05, 0.1, 0.2, 0.3.

Figure 2 Height of the cloud vs. distance x from the source for different velocities at 1m height U_r . Here ■: experimental data and calculations (curve 1) with $U_r = 0.5$ m/s; ×: experimental data and calculations (curve 2) with $U_r = 0.75$ m/s; curve 3: calculations for the case of neutrally buoyant gas and $U_r = 0.5$ m/s.

Figure 3 Similarity of the lateral and vertical dimensions of the cloud. (a) Lateral dimension of the cloud L_H vs. distance x from the source. Both L_H and x are normalized on buoyancy length scale $L_B = g_0' q_0 / U_r^3$, where $g_0^{'}$ is the initial buoyancy, q_0 is the volume flow rate of the gas in the source, U_r: wind velocity at 1m height. Curve 1: similarity relationship (33); curve 2: calculations with $U_r = 0.5$ m/s, L_B=0.058 m; curve 3 : calculations with U_r=0.75 m/s, L_B=0.017 m. (b) Parameter $\Pi_1 = (L_V' / L_V)^{1/2}$ vs. $\Pi_2 = (g'(x)/g_0')^{1/2}$, where L_V , $L_V^{'}$ are the simulated and theoretical (33) heights of the cloud, $g^{'}(x)$ is the calculated buoyancy of the cloud. Curve1: calculations with U_r=0.5 m/s; curve 2: dependence $\Pi_1 = \Pi_2$.

Figure 4 Experimental (Zhu *et al*. [4]) and calculated decay of the ground level gas concentration normalized on source gas concentration $\langle C_{vol}(x,0,0)\rangle$ with distance x for different U_r. Distance x is normalized by the length scale $L_{NM} = q^{3/5} g_0^{'1/5} / U_r$ (Neff and Meroney [41]), where $g_0^{'}$ is the initial buoyancy, q_0 is the volume flow rate of the gas in the source.

Figure 5 Experimental (Zhu *et al*. [4]) and calculated vertical profiles of (a) longitudinal component of velocity u; (b) concentration C, normalized on source gas concentration C_S; (c) turbulent intensity of the vertical component of wind velocity $\sqrt{\langle w'^2 \rangle}$ normalized on the local wind velocity $u(z)$; (d) Richardson number Ri at distance x=2.1 m from the source and $U_r = 0.5$ m/s. Symbols "•" and "○" denote the experimental data for the heavy and neutrally buoyant gas, respectively. Solid and dashed curves denote calculated data for the heavy and neutrally buoyant gas, respectively.

Figure 6 Calculated vertical profiles of the vertical turbulent momentum flux $-\langle u'' w'' \rangle$ at different distances from the source x=0.6 m (1); x=1.2 m (2); x=2.1 m (3).

Figure 7 Calculated variation of the parameter $\beta = \max_{i,j,z}\left(\left|\frac{1}{\rho}\frac{d\rho}{dt}\right| / \left(\max_k\left(\left|\frac{\partial u_k}{\partial x_k}\right|\right)\right)\right)$ with distance x from the gas source.

Figure 8 Calculated temperature distribution along wind in BURRO 8 case study at t=180 s: (a) without heat exchange with the Earth's surface; (b) taking into account the heat exchange with the surface; (c) temperature difference ($^\circ K$) between (b) and (a) cases.

Figure 9 Crosswind distribution of volume concentration in BURRO 8 case study at distance 140 m and t=180 s: (a) measurements (Koopman *et al*. [8]); (b) calculations with parameterization A; (c) calculations with parameterization B; (d) calculations with parameterization C.

Figure 10 Comparison of measured and simulated maximum centerline volume concentrations along wind in BURRO 8 case study.

Figure 11 Spatial distribution of the heat exchange coefficients in BURRO 8 experiment at *t*=100 s; (a) heat exchange coefficient of the free convection λ_2; (b) heat exchange coefficient of the forced convection λ_1. The scale λ for both coefficients is the same.

Figure 12 Dependence of the non-dimensional heat flux $\tilde{q}(t) = q(t)/q(0)$ through the Earth's surface on the non-dimensional time $\tilde{t} = tq^2(0)/\left(\rho_s c_s \chi \left(T(0,t) - T_g\right)^2\right)$ for different $\tilde{\lambda} = \lambda_2/\lambda_1$. Here, $q(t)$ is the heat flux through the surface, t is time, ρ_s, c_s, χ are density, specific heat capacity and heat conductivity of soil, respectively, $T(0,t)$ is the temperature of the Earth's surface, T_g is the constant cold gas temperature. The heat exchange coefficient $\lambda = \lambda_1 + \lambda_2$, where λ_1 and λ_2 correspond to parameterization B. Analytical solution (35) is the case of $T_g = \text{const}$, $\lambda_1 = \text{const}$, $\lambda_2 = 0$.

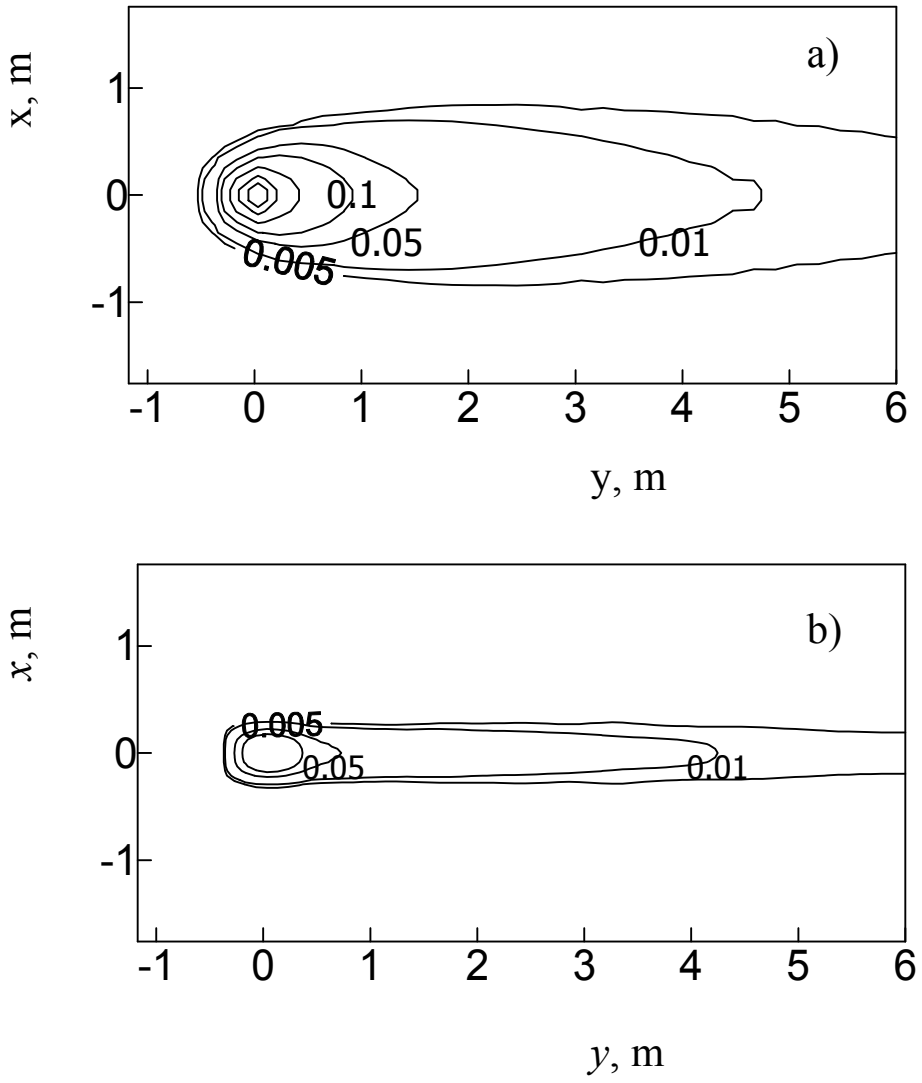

Figure 1 Calculated ground-level concentration of heavy gas (a) and neutrally buoyant gas (b) with wind velocity at 1m height $U_r = 0.5$ m/s. The isolines correspond to the values of concentration: 0.005, 0.01, 0.05, 0.1, 0.2, 0.3.

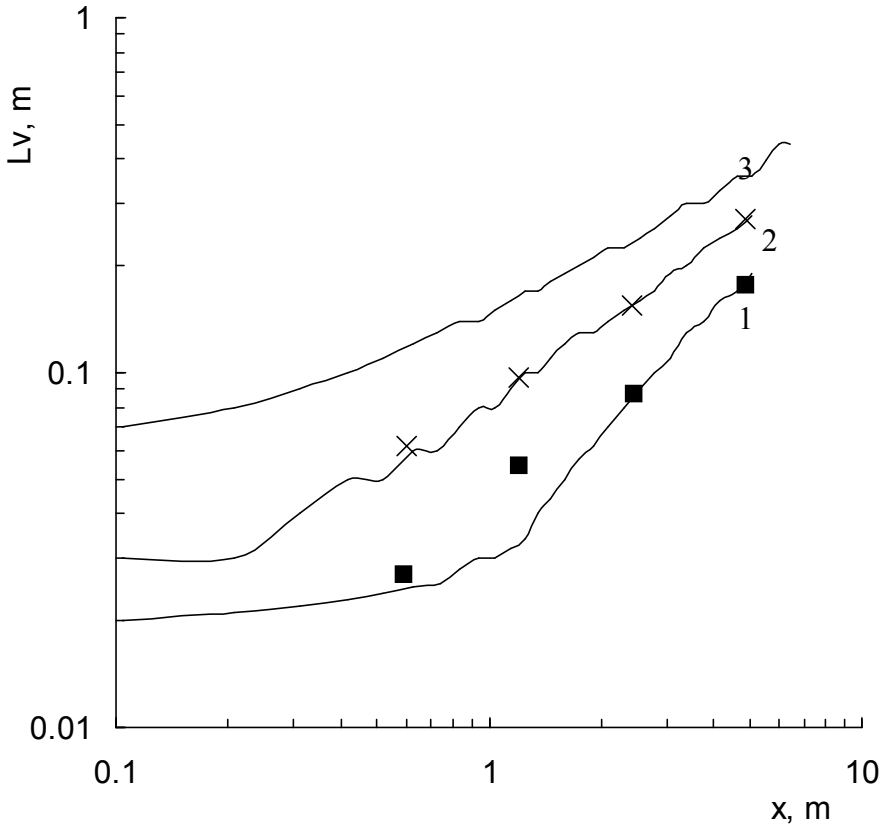

Figure 2 Height of the cloud vs. distance x from the source for different velocities at 1m height U_r . Here ■: experimental data and calculations (curve 1) with $U_r = 0.5$ m/s; ×: experimental data and calculations (curve 2) with $U_r = 0.75$ m/s; curve 3: calculations for the case of neutrally buoyant gas and $U_r = 0.5$ m/s.

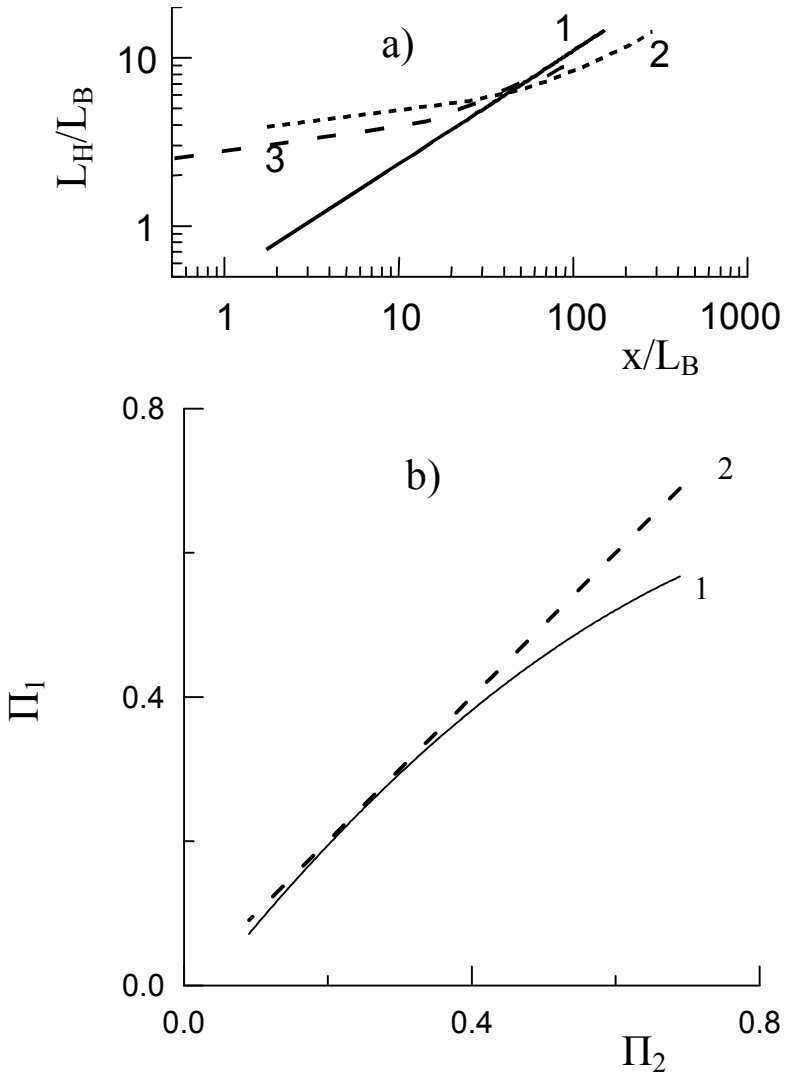

Figure 3 Similarity of the lateral and vertical dimensions of the cloud. (a) Lateral dimension of the cloud L_H vs. distance x from the source. Both L_H and x are normalized on buoyancy length scale $L_B = g_0' q_0 / U_r^3$, where g_0' is initial buoyancy, q_0 is volume flow rate of gas in the source, U_r: wind velocity at 1m height. Curve 1: similarity relationship(33); curve 2: calculations with $U_r = 0.5$ m/s, L_B=0.058 m; curve 3 : calculations with U_r=0.75 m/s, L_B=0.017 m. (b) Parameter $\Pi_1 = (L_V' / L_V)^{1/2}$ vs. $\Pi_2 = (g'(x)/g_0')^{1/2}$, where L_V, L_V' are the simulated and theoretical (33) heights of the cloud, $g'(x)$ is the calculated buoyancy of the cloud. Curve1: calculations with U_r=0.5 m/s; curve 2: dependence $\Pi_1 = \Pi_2$.

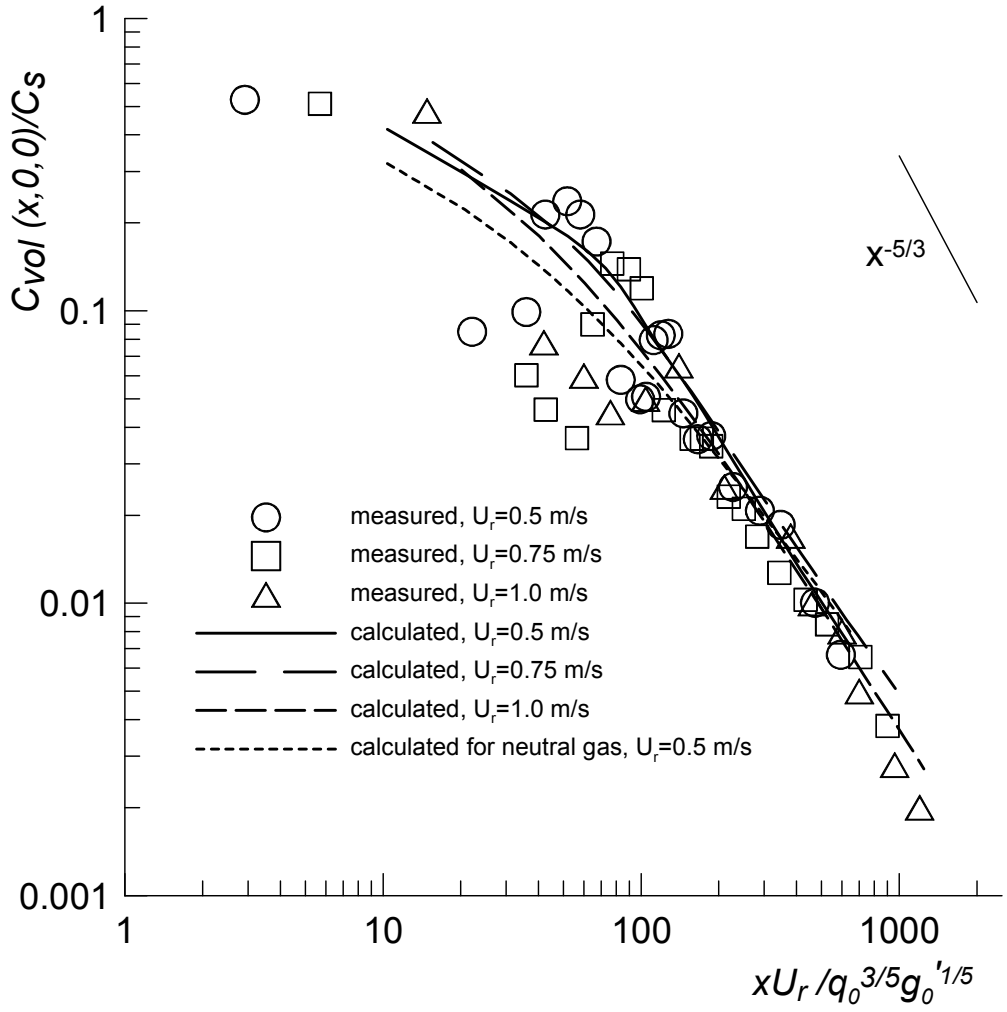

Figure 4 Experimental (Zhu *et al*. [4]) and calculated decay of the ground level gas concentration normalized on source gas concentration $\langle C_{vol}(x,0,0)\rangle$ with distance x for different U_r. Distance x is normalized by the length scale $L_{NM} = q^{3/5} g_0'^{1/5} / U_r$ (Neff and Meroney [41]), where g_0' is the initial buoyancy, q_0 is the volume flow rate of the gas in the source.

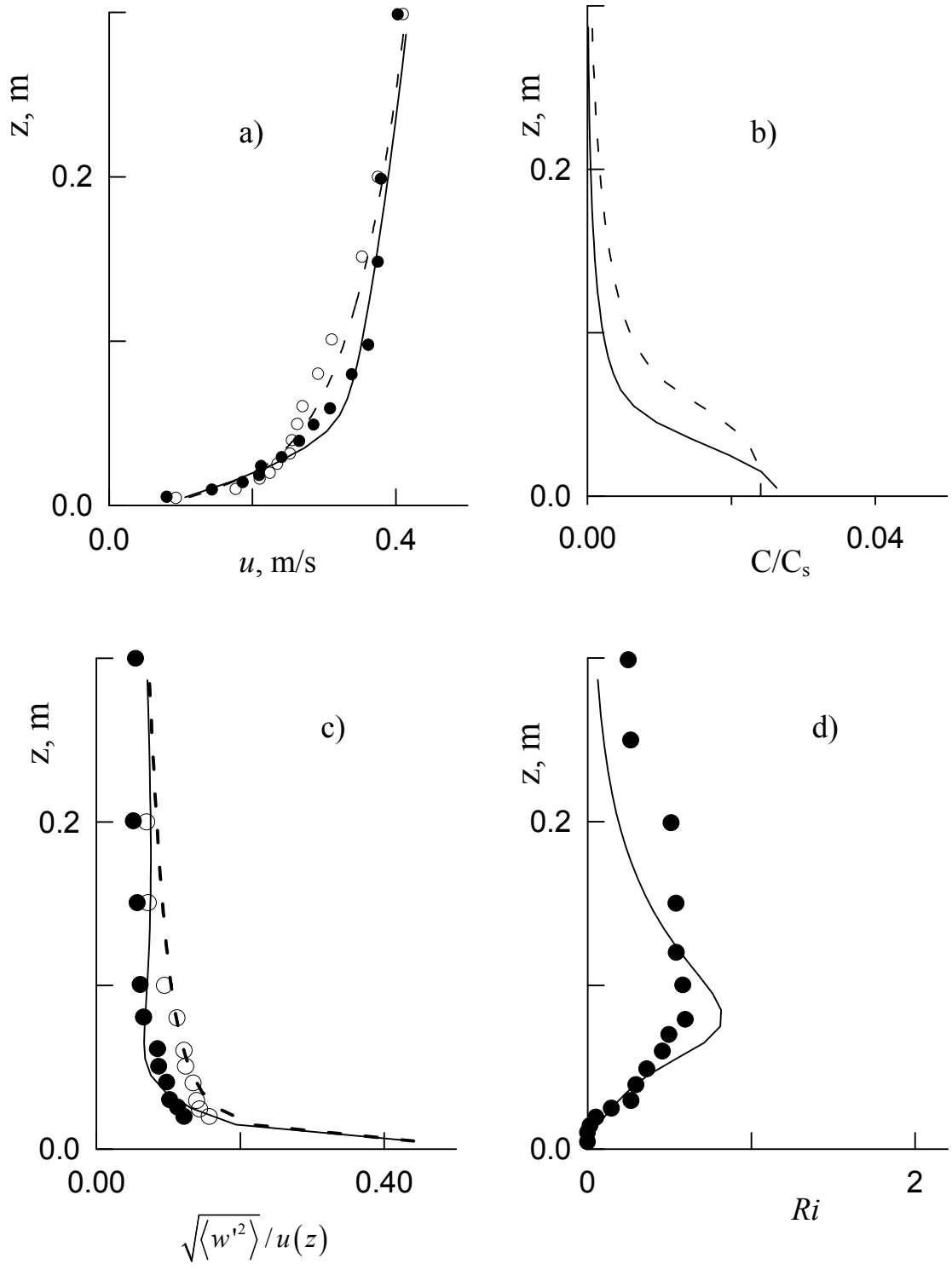

Figure 5 Experimental (Zhu *et al*. [4]) and calculated vertical profiles of (a) longitudinal component of velocity u; (b) concentration C, normalized on source gas concentration C_S; (c) turbulent intensity of the vertical component of wind velocity $\sqrt{\langle w'^2 \rangle}$ normalized on the local wind velocity $u(z)$; (d) Richardson number Ri at the distance x=2.1 m from the source and $U_r = 0.5$ m/s. Symbols "•" and "○" denote the experimental data for the heavy and neutrally buoyant gas, respectively. Solid and dashed curves denote calculated data for the heavy and neutrally buoyant gas, respectively.

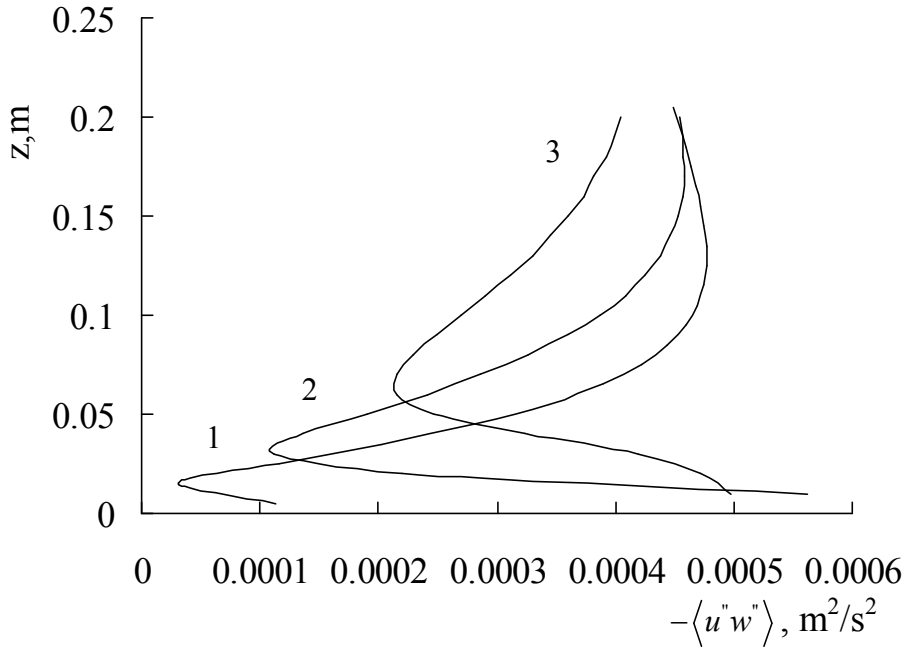

Figure 6 Calculated vertical profiles of the vertical turbulent momentum flux $-\langle u''w''\rangle$ at different distances from the source x=0.6 m (1); x=1.2 m (2); x=2.1 m (3).

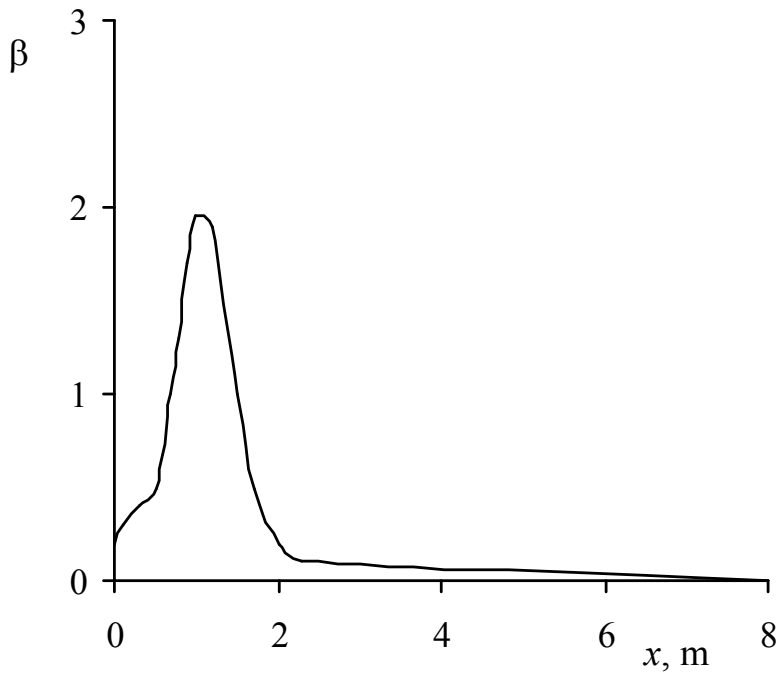

Figure 7 Calculated variation of the parameter $\beta = \max_{i,j,z}\left(\left|\frac{1}{\rho}\frac{d\rho}{dt}\right| / \left(\max_{k}\left(\left|\frac{\partial u_k}{\partial x_k}\right|\right)\right)\right)$ with distance x from the gas source.

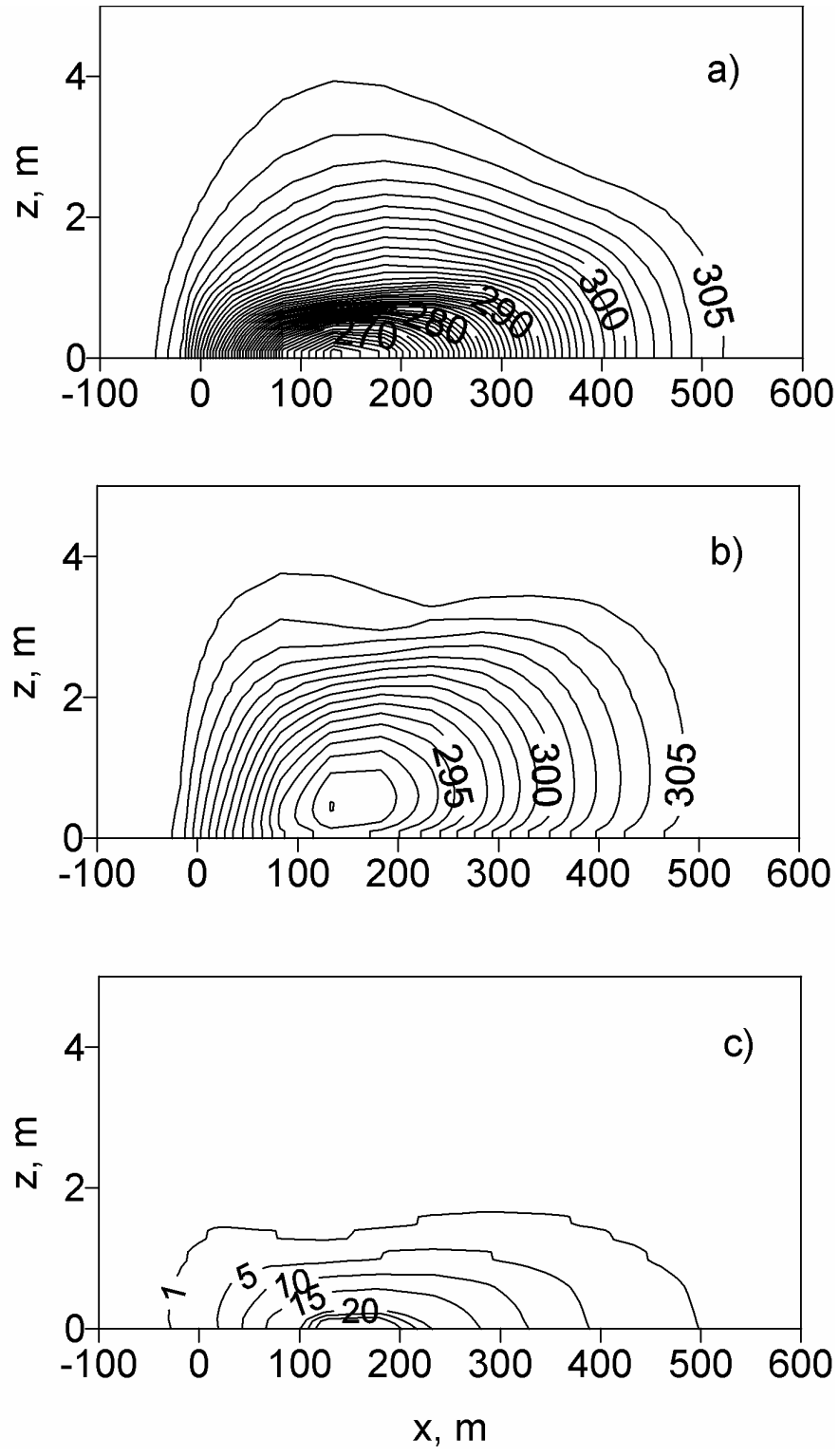

Figure 8 Calculated temperature distribution along wind in BURRO 8 case study at t=180 s: (a) without heat exchange with the Earth's surface; (b) taking into account the heat exchange with the surface; (c) temperature difference ($^{\circ}K$) between (b) and (a) cases.

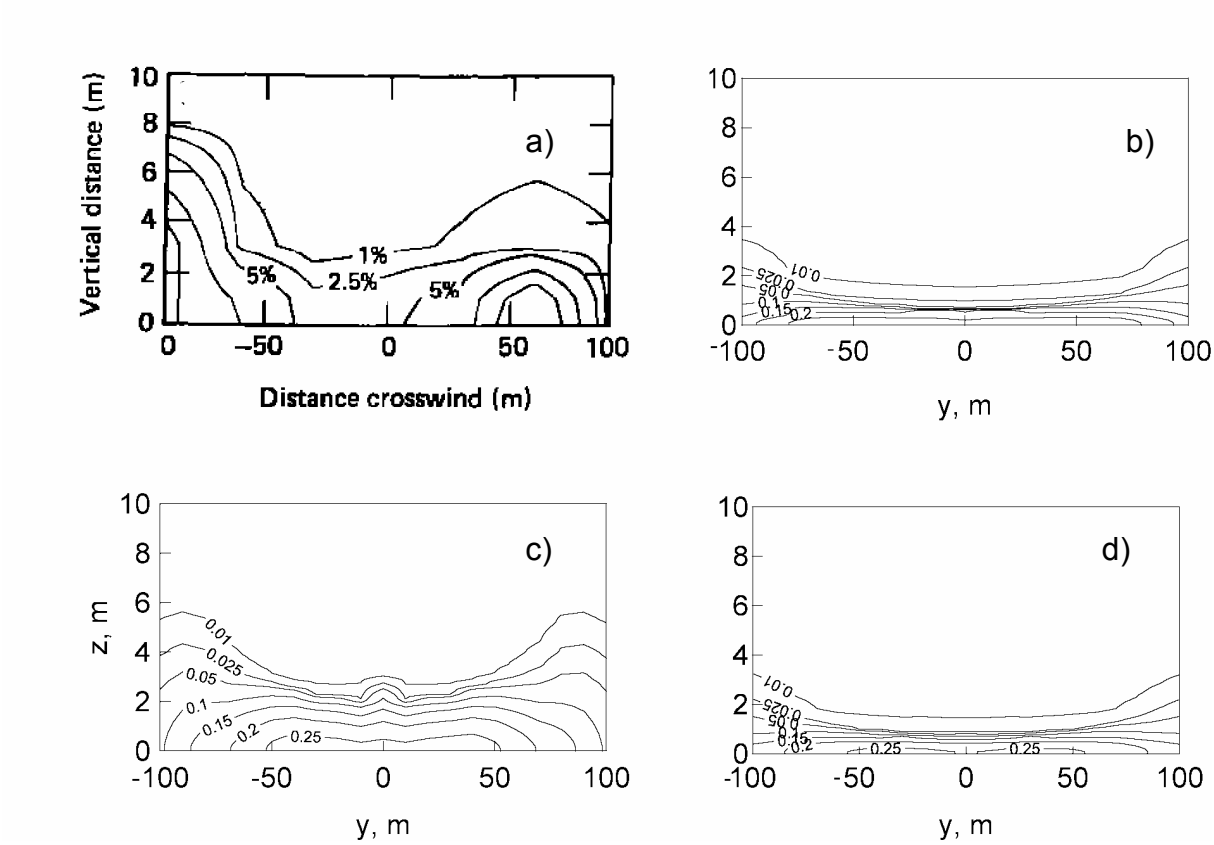

Figure 9 Crosswind distribution of volume concentration in BURRO 8 case study at distance 140 m and t=180 s: (a) measurements (Koopman et al. [8]); (b) calculations with parameterization A; (c) calculations with parameterization B; (d) calculations with parameterization C.

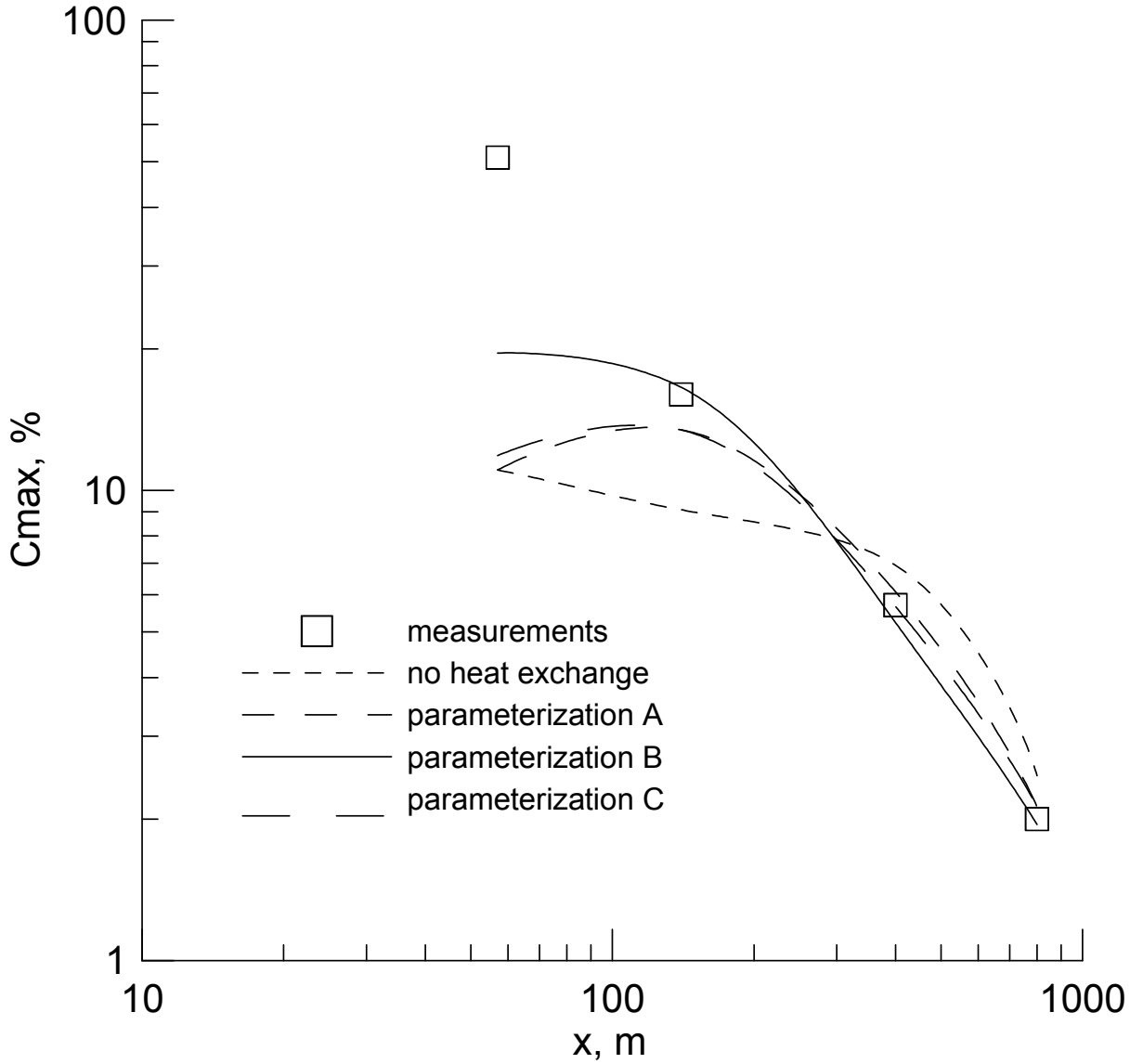

Figure 10 Comparison of measured and simulated maximum centerline volume concentrations along wind in BURRO 8 case study..

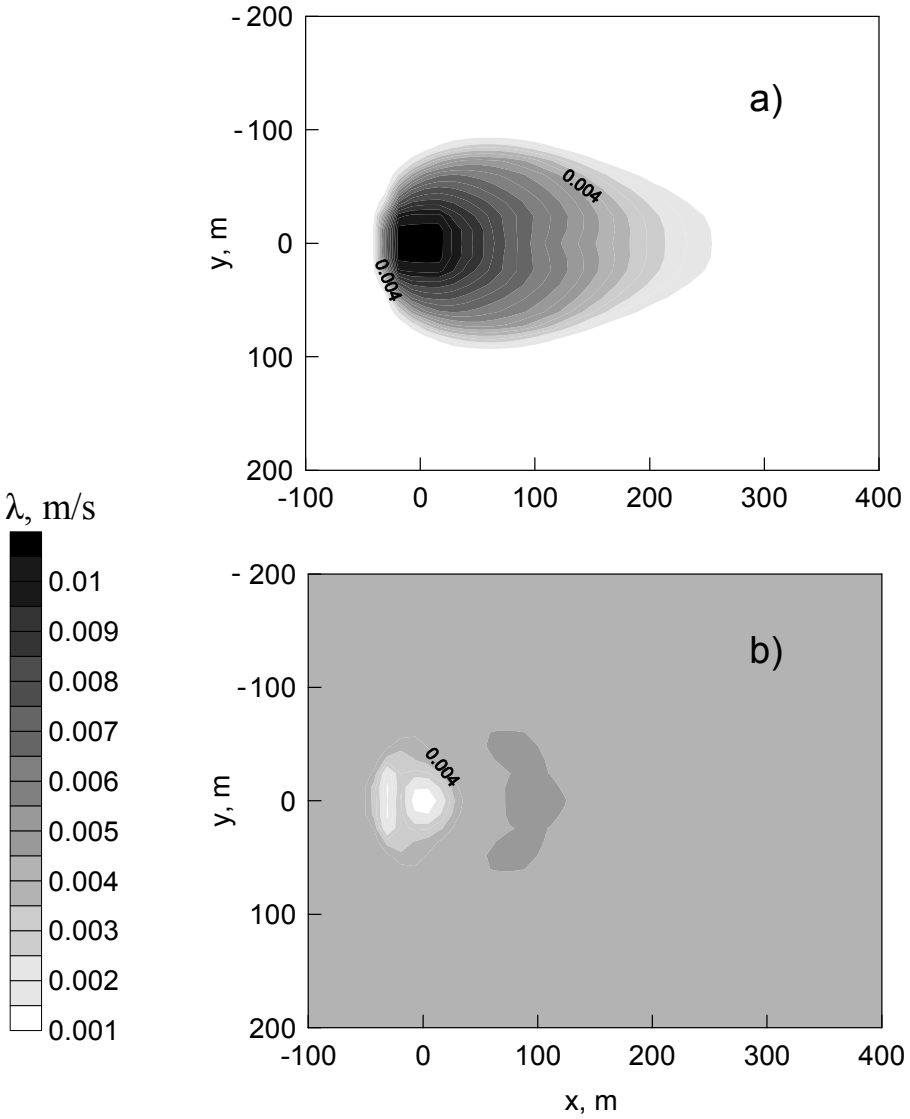

Figure 11 Spatial distribution of the heat exchange coefficients in the BURRO 8 experiment at the t=100 s; (a) heat exchange coefficient of the free convection λ_2; (b) heat exchange coefficient of the forced convection λ_1. The scale λ for both coefficient is the same.

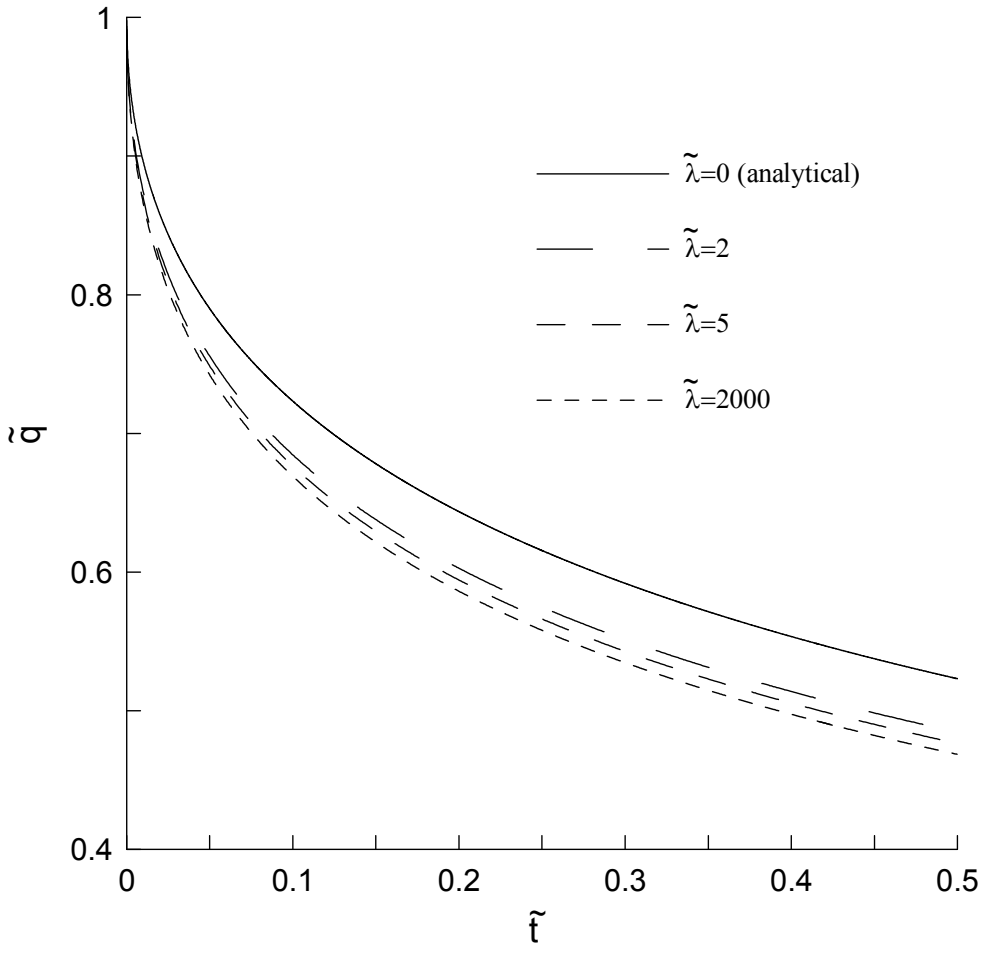

Figure 12 Dependence of the non-dimensional heat flux $\tilde{q}(t) = q(t)/q(0)$ through the Earth surface on the non-dimensional time $\tilde{t} = tq^2(0)/\left(\rho_s c_s \chi \left(T(0,t) - T_g\right)^2\right)$ for different $\tilde{\lambda} = \lambda_2/\lambda_1$. Here $q(t)$ is heat flux through the surface, t - time, ρ_s, c_s, χ - density, specific heat capacity and heat conductivity of soil, respectively, $T(0,t)$ - temperature of the Earth surface, T_g is constant cold gas temperature, heat exchange coefficient $\lambda = \lambda_1 + \lambda_2$, where λ_1 and λ_2 correspond to parameterization B. Analytical solution (35) is the case of $T_g = \text{const}$, $\lambda_1 = \text{const}$, $\lambda_2 = 0$.